EDITED BY STELLA HURTLEY

Seeing the Brain's One, Two, Three >>

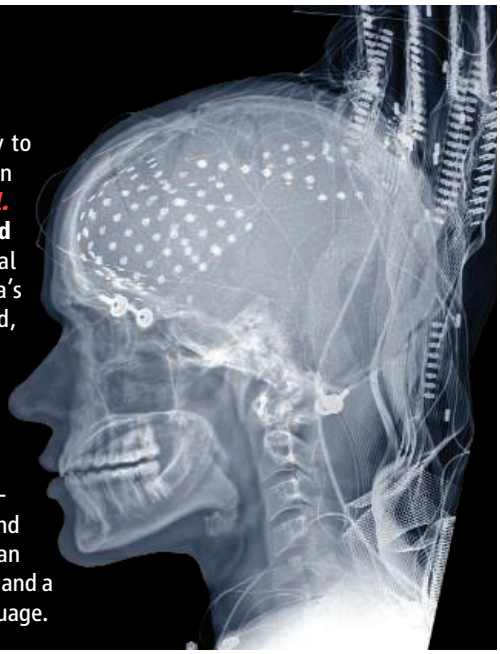

Taking advantage of the rare opportunity to record neuronal activity in the human brain using intracranial electrodes, **Sahin *et al.*** (p. 445; see the Perspective by **Hagoort and Levelt**) document the spatial and temporal pattern of neuronal populations within Broca's area as patients thought of a single word, changed its tense (for verbs) or number (for nouns), and articulated the word silently. For these three stages, they detected activity at 200, 320, and 450 milliseconds, moving in a caudal to rostral direction. These data fit neatly within the roughly 600 milliseconds required for the onset of speech and map the distinct neural computations within an area of the brain, known for almost a century and a half, as important for the production of language.

CREDITS (TOP TO BOTTOM): NED T. SAHIN/UCSD, HARVARD UNIVERSITY; SERENO *ET AL.*

Confined Germanium Thermodynamics

When a material is confined to nanoscale volumes, the very high proportion of surface to bulk can alter its thermodynamic properties. This has been studied using in situ electron microscopy, but in most cases the volume of the material is not constrained. **Holmberg *et al.*** (p. 405) studied the thermodynamics of a germanium nanowire attached to a gold seed and coated with a carbon shell to restrict its volume, measuring the reaction temperature, as well as the liquid composition without changes in volume throughout the heating cycle. This enabled monitoring of phase behavior while the germanium was being heated, and tracking solid-state diffusion across the confined interface.

Balancing the Nitrogen Budget

Setting the global budget for elements presents difficult challenges, such as accounting for possibly unknown sources or sinks. An unresolved imbalance in the oceanic nitrogen budget suggests that there may be additional sources of biological nitrogen fixation in the deep sea. Using high-resolution imaging techniques, **Dekas *et al.*** (p. 422; see the Perspective by **Fulweiler**) observed direct assimilation of isotopically labeled N_2 by anaerobic methane-oxidizing archaea from deep marine sediment and the subsequent transfer of nitrogen to their sulfate-reducing bacterial symbionts. This slow and energetically costly conversion by archaea is dependent upon methane and requires physical contact with the associated bacterial partner. Such syntrophic consortia represent a potential source of nitrogen in the oceans and may help to balance the global nitrogen budget.

Like Beads on a String

The optimal packing of spheres, and the somewhat lower densities obtained in the compaction of granular materials are well studied problems. What is less clear is what happens when the spheres are connected, as in the case of polymeric materials—often represented by connected sphere models. **Zou *et al.*** (p. 408; see the Perspective by **Reichhardt and Lopatina**) examined the packing of chains of metal beads commonly used for securing bathroom drain plugs or for raising or lowering window blinds. Both the length of the chains, and whether they were linear or looped, influenced the overall packing density. Jamming the chains together captured the key physics of the glass transition of polymeric materials.

Magnetic Monopoles

Magnets come with a north and a south pole. Despite being predicted to exist, searches in astronomy and in high-energy particle physics experiments for magnetic monopoles (either north or south on their own) have defied observation. Theoretical work in condensed-matter systems has predicted that spin-ice structures may harbor such elusive particles (see the Perspective by **Gingras**). **Fennell *et al.*** (p. 415, published online 3 September) and **Morris *et al.*** (p. 411, published online 3 September) used polarized neutron scattering to probe the spin structure forming in two spin-ice compounds—$Ho_2Ti_2O_7$ and $Dy_2Ti_2O_7$—and present results in support of the presence of magnetic monopoles in both materials.

Haploid Medaka Stem Cells

Although diploid embryonic stem cells have been generated by various means, there would also be value in deriving haploid stem cells. In these cells, recessive mutations in essential genes would show phenotypes that would not be apparent in heterozygous animals. **Yi *et al.*** (p. 430) used the medaka fish model system to generate haploid stem cells that show stable growth and pluripotency. In addition, a fertile female medaka fish was produced by haploid embryonic stem cell nuclear transfer into a normal egg. This system has potential for analyzing recessive genes, for example, in disease phenotypes or in various cell lineages in culture.

Diddy Dinosaurs

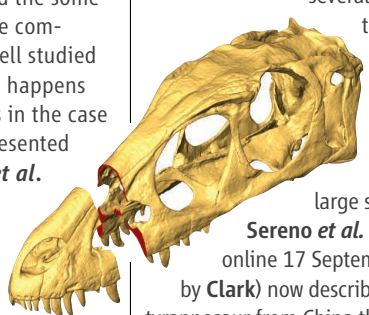

Tyrannosaurs were the dominant large dinosaur predator during the Late Cretaceous. They have several distinct specialized features, including an oversized skull, huge hindlimbs, and tiny arms, that have been thought to have evolved in concert with their large size and carnivorous diet. **Sereno *et al.*** (p. 418, published online 17 September; see the Perspective by **Clark**) now describe an earlier, diminutive tyrannosaur from China that also has these common specializations. Thus, these features were not a result of size increase but appear to have been required for feeding efficiency at all sizes.

Coupling Clocks and Metabolism

Circadian clocks in mammals coordinate behavior and physiology with daily light-dark cycles by driving rhythmic transcription of thousands of genes. The master clock in the brain is set by light, but clocks in peripheral tissues, such as the liver, are set by daily feeding. Such coupling should allow tissues to "anticipate" food

Continued on page 337

Published by AAAS

NEUROSCIENCE

The Speaking Brain

Recordings of electrical activity in the human brain reveal the fine-tuned, stepwise neuronal processing of language and speech.

Peter Hagoort[1,2] and Willem J. M. Levelt[1]

How does intention to speak become the action of speaking? It involves the generation of a preverbal message that is tailored to the requirements of a particular language, and through a series of steps, the message is transformed into a linear sequence of speech sounds (*1*, *2*). These steps include retrieving different kinds of information from memory (semantic, syntactic, and phonological), and combining them into larger structures, a process called unification. Despite general agreement about the steps that connect intention to articulation, there is no consensus about their temporal profile or the role of feedback from later steps (*3*, *4*). In addition, since the discovery by the French physician Pierre Paul Broca (in 1865) of the role of the left inferior frontal cortex in speaking, relatively little progress has been made in understanding the neural infrastructure that supports speech production (*5*). One reason is that the characteristics of natural language are uniquely human, and thus the neurobiology of language lacks an adequate animal model. But on page 445 of this issue, Sahin *et al*. (*6*) demonstrate, by recording neuronal activity in the human brain, that different kinds of linguistic information are indeed sequentially processed within Broca's area.

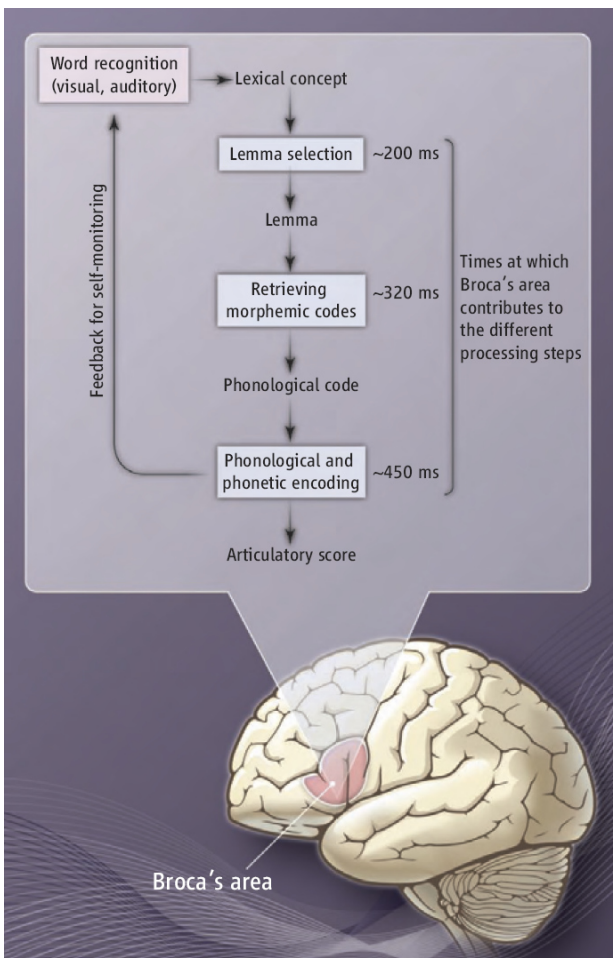

From intention to articulation. Shown is an adapted version of the lexical encoding model for speech production (*2*), specifying steps in the paradigm used by Sahin *et al*. Based on the visual input, a lemma is selected that specifies the syntactic features of a lexical concept. For instance, for the lemma *horse*, it specifies that it is a count noun. In addition, the morphemic codes are retrieved. For instance, when the speaker wants to produce the plural form of *horse*, the codes for both the stem and the plural suffix are retrieved. Next, the phonological codes for each morpheme are retrieved, combined, and transformed into a motor command to the articulatory system. The approximate times (in milliseconds) at which Broca's area contributes to the different processing steps are shown. The late (i.e., at 500 to 600 ms) monophasic component observed in the temporal lobe (*6*) might reflect self-monitoring of the speech output.

Sahin *et al*. had the unique opportunity to record from three patients with epilepsy during presurgical preparation. Depth electrodes were implanted in Broca's area and the anterior temporal cortex, and local field potentials were recorded while the patients were engaged in a language production task. The subjects were asked either to read silently words presented on a screen, or to silently produce the inflected form of the presented nouns and verbs in accordance with the syntactic requirements imposed by a short sentence fragment (e.g., Yesterday they… walked). This latter process has two components (see the figure). One is to determine the correct tense of the target word and to generate (for regular inflections) or retrieve (for irregular inflections) the correct morphological form. The other is the generation of the concomitant phonological code and preparation for articulation.

Particularly in Broca's area, more specifically Brodmann area 45, a clear triphasic local field potential response was observed. At about 200 ms after presentation of the word, word identification had taken place, with a stronger response for low-frequency words than for high-frequency words. Morphological composition and retrieval for nouns and verbs happened at around 320 ms. Finally, at about 450 ms, phonological encoding had been completed. All these operations were not only temporally separated, but also spatially segregated at a scale of only a few millimeters, which is below the effective spatial resolution of standard functional magnetic resonance imaging of brain activity.

These data are relevant for both cognitive models of speech production and for accounts on the role of Broca's area. The time course is clear evidence for the sequentiality of different access and unification operations in speaking, and is consistent with the few estimates in the literature (*7*, *8*). Moreover, both the anatomical and the temporal segregation of word-encoding operations in Broca's area are in line with the view that this region is involved with each of these encoding operations and their unification over time. Feedback operations among these processes cannot be excluded. However, the fine-grained temporal and spatial separation of these steps suggests that we are witnessing the "first go" process at work here.

Both functional magnetic resonance imaging and lesion studies have shown that Broca's area is also involved in processing inflectional morphology during comprehension (*9*). In combination with the findings of Sahin *et al*., this suggests that Broca's area is recruited during both language production and comprehension. Whether these recruitments can be separated at the scale of the microcircuitry within Broca's area remains to be seen.

Broca's area has been proposed to have a more specialized role in language processing—facilitating linguistically motivated operations of syntactic movement (*10*) and processing hierarchical structures (*11*). The

[1]Max Planck Institute for Psycholinguistics, NL-6500 HB Nijmegen, Netherlands. [2]Donders Institute for Brain, Cognition and Behaviour, Radboud University Nijmegen, Netherlands. E-mail: peter.hagoort@donders.ru.nl

results of Sahin *et al*. indicate that the role of Broca's area is not so limited, but should be characterized in more general terms. It is likely involved in unification operations at the word and sentence level, in connection with temporal regions that are crucial for memory retrieval (*12*).

As is known for neurons in the visual cortex (*13*), the specific contribution of Broca's area may well vary with time, as a consequence of the different dynamic cortical networks in which it is embedded at different time slices. This fits well with the finding that Broca's area is not language specific, but is also recruited in the service of other cognitive domains, such as music (*14*) and action (*15*), and with the finding that its contribution to language processing crosses the boundaries of semantics, syntax, and phonology.

References

1. W. J. M. Levelt, *Speaking: From Intention to Articulation* (MIT Press, Cambridge, MA, 1989).
2. W. J. M. Levelt, *Proc. Natl. Acad. Sci. U.S.A.* **98**, 13464 (2001).
3. W. J. M. Levelt, A. Roelofs, A. S. Meyer, *Behav. Brain Sci.* **22**, 1 (1999).
4. G. S. Dell, M. F. Schwartz, N. Martin, E. M. Saffran, D. A. Gagnon, *Psychol. Rev.* **104**, 801 (1997).
5. P. Broca, *Bull. Soc. Anthropol. Paris* **6**, 377 (1865).
6. N. T. Sahin, S. Pinker, S. S. Cash, D. Schomer, E. Halgren, *Science* **326**, 445 (2009).
7. P. Hagoort, M. van Turennout, in *Speech Motor Production and Fluency Disorders: Brain Research in Speech Production*, W. Hulstijn, H. Peters, P. Van Lieshout, Eds. (Elsevier, Amsterdam, 1997), pp. 351–361.
8. P. Indefrey, W. J. M. Levelt, *Cognition* **92**, 101 (2004).
9. L. K. Tyler, W. Marslen-Wilson, *Philos. Trans. R. Soc.* **363**, 1037 (2008).
10. Y. Grodzinsky, A. Santi, *Trends Cogn. Sci.* **12**, 474 (2008).
11. A. D. Friederici, *Trends Cogn. Sci.* **8**, 245 (2004).
12. P. Hagoort, *Trends Cogn. Sci.* **9**, 416 (2005).
13. V. A. Lamme, P. R. Roelfsema, *Trends Neurosci.* **23**, 571 (2000).
14. A. D. Patel, *Nat. Neurosci.* **6**, 674 (2003).
15. F. Hamzei *et al*., *Neuroimage* **19**, 637 (2003).

10.1126/science.1181675

PALEONTOLOGY

Becoming *T. rex*

A small tyrannosaur from the Early Cretaceous sheds light on the origin of predatory features of *Tyrannosaurus rex*.

James Clark

Gigantic, ferocious, long-dead animals like *Tyrannosaurus rex* never fail to capture people's attention, and the discovery of a new tyrannosaur—giant or otherwise—is always big news. On page 418 of this issue, Sereno *et al*. (*1*) report on a spectacular skeleton of a new genus and species near the ancestry of the group including *T. rex* and its closest relatives, the Tyrannosauridae. At an estimated 3 m total length, *Raptorex kriegsteini* is much smaller than the largest *T. rex* [12.8 m long (*2*)] and other tyrannosaurids, but has several key features previously known only in this family. *Raptorex* thus provides a glimpse at how tyrannosaurids evolved.

Department of Biological Sciences, George Washington University, Washington, DC 20052, USA. E-mail: jclark@gwu.edu

Fossils preserved in the rock with *Raptorex* point strongly to its origin from the beds at the bottom of the Jehol Group in northeastern China, although the locality remains unknown. The Jehol Group fossil beds (*3*) are famous for preserving dinosaurs with feathers in their thin-bedded shales, including the basal tyrannosaur *Dilong* (*4*), but the skeletons are usually crushed into two dimensions, and structures such as the skull are difficult to study. Fortunately, a series of beds in the lowest part of the Jehol Group yields exquisitely preserved, uncrushed skeletons, albeit without any soft tissues.

The *Raptorex* specimen was purchased a few years ago by Henry J. Kriegstein at the Tucson Gem and Mineral Show (*5*), a venue notorious for the sale of illegally collected fossils, such as the famous *Archaeoraptor* chimera from the Jehol Group (*6*). Kriegstein approached Sereno with the fossil, and Sereno agreed to describe it on the condition that it would be deposited in a collection in China (*5*). Although the fossil is currently with Sereno in Chicago, the specimen will be deposited in the Long Hao Institute of Geology and Paleontology in Hohhot, Inner Mongolia. Lin Tan of that institute is a coauthor of the paper, along with Kriegstein.

What to do with "hot" specimens is a conundrum for scientists. Such specimens almost always lack reliable locality data and therefore information about the sediments in which they were preserved. Stolen fossils can preserve data about the anatomy of a new or poorly known species, but enriching thieves or their fences is no more ethical for a fossil than for a car or a Grecian statue. The naming of a new ankylosaur, *Minotaurasaurus ramachandrani* (*7*), was strongly criticized (*8*), because the fossil was almost certainly

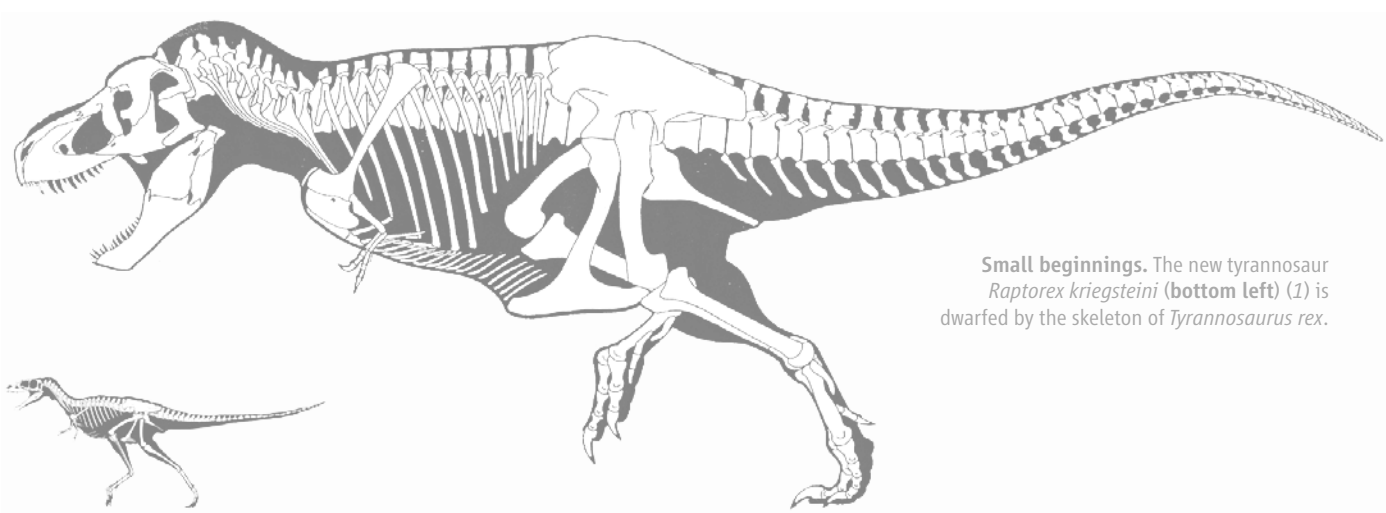

Small beginnings. The new tyrannosaur *Raptorex kriegsteini* (**bottom left**) (*1*) is dwarfed by the skeleton of *Tyrannosaurus rex*.

CREDITS: *RAPTOREX* SKELETON MODIFIED FROM (*1*); *T. REX* SKELETON BY G. S. PAUL

the basic taste modalities is mediated by distinct TRCs, with taste at the periphery proposed to be encoded via labeled lines [i.e., a sweet line, a sour line, a bitter line, etc. (*21*)]. Given that Car4 is specifically tethered to the surface of sour-sensing cells, and thus ideally poised to provide a highly localized acid signal to the sour TRCs, we reasoned that carbonation might be sensed through activation of the sour-labeled line. A prediction of this postulate is that prevention of sour cell activation should eliminate CO_2 detection, even in the presence of wild-type Car4 function. To test this hypothesis, we engineered animals in which the activation of nerve fibers innervating sour-sensing cells was blocked by preventing neurotransmitter release from the PKD2L1-expressing TRCs. In essence, we transgenically targeted expression of tetanus toxin light chain [TeNT, an endopeptidase that removes an essential component of the synaptic machinery (*34*–*36*)] to sour-sensing TRCs, and then monitored the physiological responses of these mice to sweet, sour, bitter, salty, umami and CO_2 stimulation. As predicted, taste responses to sour stimuli were selectively and completely abolished, whereas responses to sweet, bitter, salty and umami tastants remained unaltered (Fig. 4 and fig. S5). However, these animals also displayed a complete loss of taste responses to CO_2 even though they still expressed Car4 on the surface of PKD2L1 cells. Together, these results implicate the extracellular generation of protons, rather than intracellular acidification (*15*), as the primary signal that mediates the taste of CO_2, and demonstrate that sour cells not only provide the membrane anchor for Car4 but also serve as the cellular sensors for carbonation.

Why do animals need CO_2 sensing? CO_2 detection could have evolved as a mechanism to recognize CO_2-producing sources (*18*, *37*)—for instance, to avoid fermenting foods. This view would be consistent with the recent discovery of a specialized CO_2 taste detection in insects where it mediates robust innate taste behaviors (*38*). Alternatively, Car4 may be important to maintain the pH balance within taste buds, and might gratuitously function as a detector for carbonation only as an accidental consequence. Although CO_2 activates the sour-sensing cells, it does not simply taste sour to humans. CO_2 (like acid) acts not only on the taste system but also in other orosensory pathways, including robust stimulation of the somatosensory system (*17*, *22*); thus, the final percept of carbonation is likely to be a combination of multiple sensory inputs. Nonetheless, the "fizz" and "tingle" of heavily carbonated water is often likened to mild acid stimulation of the tongue, and in some cultures seltzer is even named for its salient sour taste (e.g., saurer Sprudel or Sauerwasser).

References and Notes

1. G. Nelson *et al.*, *Cell* **106**, 381 (2001).
2. G. Nelson *et al.*, *Nature* **416**, 199 (2002).
3. X. Li *et al.*, *Proc. Natl. Acad. Sci. U.S.A.* **99**, 4692 (2002).
4. E. Adler *et al.*, *Cell* **100**, 693 (2000).
5. J. Chandrashekar *et al.*, *Cell* **100**, 703 (2000).
6. H. Matsunami, J. P. Montmayeur, L. B. Buck, *Nature* **404**, 601 (2000).
7. K. L. Mueller *et al.*, *Nature* **434**, 225 (2005).
8. A. L. Huang *et al.*, *Nature* **442**, 934 (2006).
9. Y. Ishimaru *et al.*, *Proc. Natl. Acad. Sci. U.S.A.* **103**, 12569 (2006).
10. N. D. Lopezjimenez *et al.*, *J. Neurochem.* **98**, 68 (2006).
11. Y. Zhang *et al.*, *Cell* **112**, 293 (2003).
12. G. Q. Zhao *et al.*, *Cell* **115**, 255 (2003).
13. A. A. Kawamura, in *Olfaction and Taste II*, T. Hayashi, Ed. (Pergamon, New York, 1967), pp. 431–437.
14. M. Komai, B. P. Bryant, T. Takeda, H. Suzuki, S. Kimura, in *Olfaction and Taste XI*, K. Kurihara, N. Suzuki, H. Ogawa, Eds. (Springer-Verlag, Tokyo, 1994), pp. 92.
15. V. Lyall *et al.*, *Am. J. Physiol. Cell Physiol.* **281**, C1005 (2001).
16. J. M. Dessirier, C. T. Simons, M. O'Mahony, E. Carstens, *Chem. Senses* **26**, 639 (2001).
17. C. T. Simons, J. M. Dessirier, M. I. Carstens, M. O'Mahony, E. Carstens, *J. Neurosci.* **19**, 8134 (1999).
18. J. Hu *et al.*, *Science* **317**, 953 (2007).
19. S. Lahiri, R. E. Forster 2nd, *Int. J. Biochem. Cell Biol.* **35**, 1413 (2003).
20. M. Dahl, R. P. Erickson, S. A. Simon, *Brain Res.* **756**, 22 (1997).
21. J. Chandrashekar, M. A. Hoon, N. J. Ryba, C. S. Zuker, *Nature* **444**, 288 (2006).
22. M. Komai, B. P. Bryant, *Brain Res.* **612**, 122 (1993).
23. L. G. Miller, S. M. Miller, *J. Fam. Pract.* **31**, 199 (1990).
24. M. Graber, S. Kelleher, *Am. J. Med.* **84**, 979 (1988).
25. D. Brown, L. M. Garcia-Segura, L. Orci, *Brain Res.* **324**, 346 (1984).
26. H. Daikoku *et al.*, *Chem. Senses* **24**, 255 (1999).
27. B. Bottger, T. E. Finger, B. Bryant, *Chem. Senses* **21**, 580 (1996).
28. Y. Akiba *et al.*, *Gut* **57**, 1654 (2008).
29. C. T. Supuran, *Curr. Pharm. Des.* **14**, 603 (2008).
30. W. S. Sly, P. Y. Hu, *Annu. Rev. Biochem.* **64**, 375 (1995).
31. T. Okuyama, A. Waheed, W. Kusumoto, X. L. Zhu, W. S. Sly, *Arch. Biochem. Biophys.* **320**, 315 (1995).
32. G. N. Shah *et al.*, *Proc. Natl. Acad. Sci. U.S.A.* **102**, 16771 (2005).
33. D. Vullo *et al.*, *Bioorg. Med. Chem. Lett.* **15**, 971 (2005).
34. M. Yamamoto *et al.*, *J. Neurosci.* **23**, 6759 (2003).
35. C. R. Yu *et al.*, *Neuron* **42**, 553 (2004).
36. Y. Zhang *et al.*, *Neuron* **60**, 84 (2008).
37. G. S. Suh *et al.*, *Nature* **431**, 854 (2004).
38. W. Fischler, P. Kong, S. Marella, K. Scott, *Nature* **448**, 1054 (2007).

39. We thank W. Guo and A. Becker for generation and maintenance of mouse lines, M. Hoon for help in the initial phase of this work, E. R. Swenson for a generous gift of benzolamide, M. Goulding for *Rosa26-flox-STOP-TeNT* mice, A. Waheed for Car4 antibodies, and members of the Zuker laboratory for valuable comments. Supported in part by the intramural research program of the NIH, NIDCR (N.J.P.R.). C.S.Z. is an investigator of the Howard Hughes Medical Institute.

Supporting Online Material

www.sciencemag.org/cgi/content/full/326/5951/443/DC1
Materials and Methods
Figs. S1 to S5
References

6 April 2009; accepted 17 August 2009
10.1126/science.1174601

Sequential Processing of Lexical, Grammatical, and Phonological Information Within Broca's Area

Ned T. Sahin,[1,2]* Steven Pinker,[2] Sydney S. Cash,[3] Donald Schomer,[4] Eric Halgren[1]

Words, grammar, and phonology are linguistically distinct, yet their neural substrates are difficult to distinguish in macroscopic brain regions. We investigated whether they can be separated in time and space at the circuit level using intracranial electrophysiology (ICE), namely by recording local field potentials from populations of neurons using electrodes implanted in language-related brain regions while people read words verbatim or grammatically inflected them (present/past or singular/plural). Neighboring probes within Broca's area revealed distinct neuronal activity for lexical (~200 milliseconds), grammatical (~320 milliseconds), and phonological (~450 milliseconds) processing, identically for nouns and verbs, in a region activated in the same patients and task in functional magnetic resonance imaging. This suggests that a linguistic processing sequence predicted on computational grounds is implemented in the brain in fine-grained spatiotemporally patterned activity.

Within cognitive neuroscience, language is understood far less well than sensation, memory, or motor control, because language has no animal homologs, and methods appropriate to humans [functional magnetic resonance imaging (fMRI), studies of brain-damaged patients, and scalp-recorded potentials] are far coarser in space or time than the underlying causal events in neural circuitry. Moreover, language involves several kinds of abstract information (lexical, grammatical, and phonological) that are difficult to manipulate independently. This has left a gap in understanding between the computational structure of language suggested by linguistics and the neural circuitry that implements language processing. We narrow this gap using a technique with high spatial, temporal, and physiological resolution and a task that distinguishes three components of linguistic computation.

According to linguistic analyses, the ability to identify words, combine them grammatically, and articulate their sounds involves several kinds of

[1]Department of Radiology, University of California–San Diego, La Jolla, CA 92037, USA. [2]Department of Psychology, Harvard University, Cambridge, MA 02138, USA. [3]Department of Neurology, Massachusetts General Hospital, Boston, MA 02114, USA. [4]Department of Neurology, Beth Israel Deaconess Medical Center, Boston, MA 02215, USA.

*To whom correspondence should be addressed. E-mail: sahin@post.harvard.edu

representations, with logical dependencies among them (*1*, *2*). For example, to pronounce a verb in a sentence, one must determine the appropriate tense given the intended meaning and syntactic context (e.g., "walk," "walks," "walked," or "walking"). One must identify the particular verb, which specifies whether to use a regular (e.g., "walked") or irregular (e.g., "went") form. In addition, one must unpack the phonological content of the verb and suffix to implement three more computations: phonological adjustments in the sequence of phonemes (e.g., inserting a vowel between verb and suffix in "patted" but not in "walked"), phonetic adjustments in the pronunciation of the phonemes (such as the difference between the "d" in "walked" and "jogged"), and conversion of the phoneme sequence into articulatory motor commands.

This logical decomposition does not entail that each kind of representation corresponds to a distinct stage or circuit in the brain. In many neural-network models, the selection of tense, discrimination of regular from irregular inflection, and formulation of the phonetic output are computed in parallel and in one time-step within a single distributed network (*3*, *4*). Others contain loops and feedback connections, propagate probabilistic constraints, and iteratively settle into a globally stable state, with no fixed sequence of operations (*5*). Even stage models may incorporate cascades where partial information from one stage begins to feed the next before its computation is complete (*6*). Nonetheless, the most comprehensive model of speech production, developed by Levelt, Roelofs, and Meyer (LRM), maximizes parsimony and falsifiability by implementing linguistic operations as discrete ordered stages, eschewing feedback, loops, parallelism, or cascades (*7*). They posit stages for lexical retrieval (which they associate with the left middle temporal gyrus at 150 to 225 ms after stimulus presentation), grammatical encoding (locus and duration unknown), phonological retrieval (posterior temporal lobe, 200 to 400 ms), phonological and phonetic processing (Broca's area, 400 to 600 ms), self-monitoring (superior temporal lobe, beginning at 275 to 400 ms but highly variable in duration), and articulation (motor cortex) (*8*, *9*).

Current evidence, however, leaves considerable uncertainty about the localization and timing of these components, especially grammatical processing. Although clinical studies report double dissociations in which a patient is more impaired in grammar than phonology or vice versa (*10*), in most studies both abilities are linked to similar regions in the left inferior prefrontal cortex, particularly Broca's area (*11*). Although Broca's area itself has been identified as the seat of phonology, grammar, and even specific grammatical operations (*12*–*14*), lesion and neuroimaging

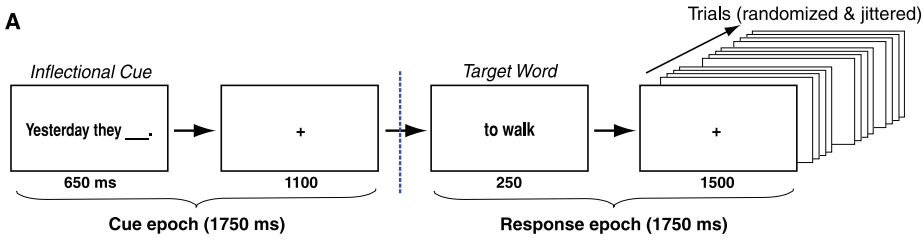

B

Condition	Examples [Verbs]	Examples [Nouns]	Requires Inflection	Change in Phonology
Read	repeat word: ___. (response = "*walk*")	repeat word: ___. ("*rock*")	X	X
Null-Inflect	Every day they ___. ("*walk*")	That is the ___. ("*rock*")	✓	X
Overt-Inflect	Yesterday they ___. ("*walked*")	Those are the ___. ("*rocks*")	✓	✓

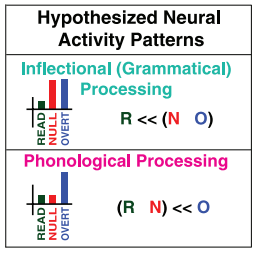

Fig. 1. Experimental design. (**A**) Structure of trials. (**B**) Experimental conditions, example trials, and required psycholinguistic processes. (**C**) Hypothesized patterns of neural activity by condition, for inflectional and phonological processing.

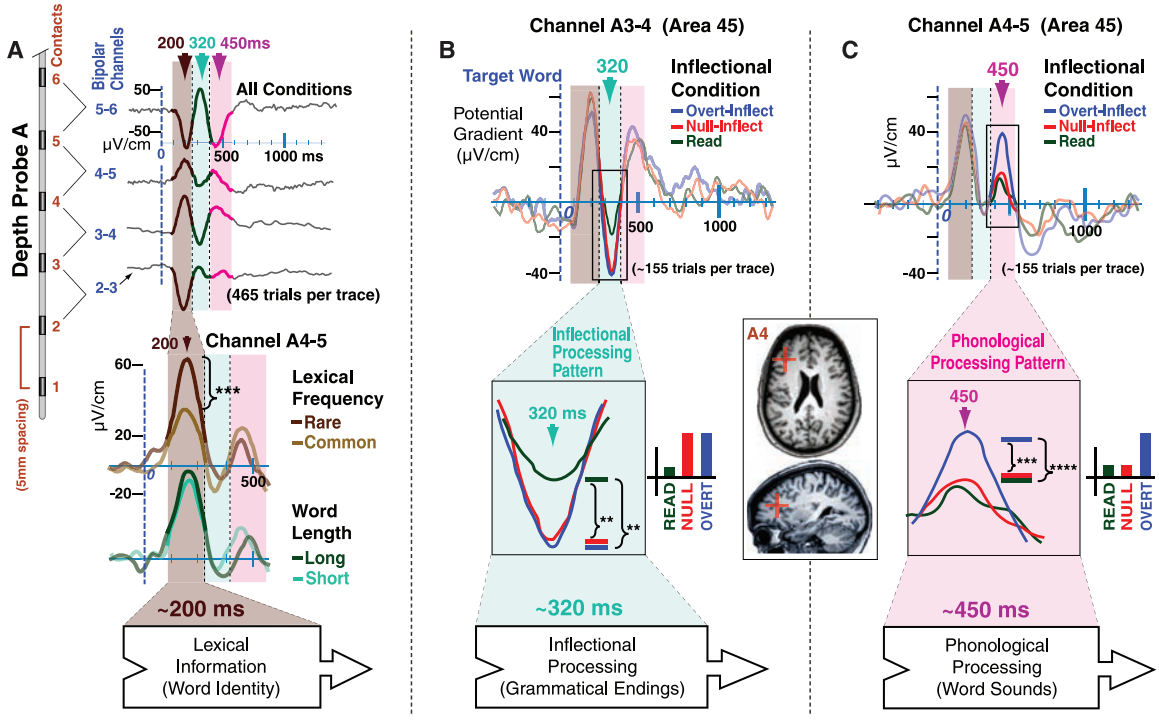

Fig. 2. (**A**) Main results: sequential processing of lexical, grammatical, and phonological information in overlapping circuits. (Top) Neural activity recorded from several channels in Broca's area (patient A, Brodmann area 45) shows three LFP components that were consistently evoked by the task (~200, ~320, and ~450 ms). (Bottom) The ~200-ms component is sensitive to word frequency but not word length, suggesting that it indexes a cognitive process such as lexical identification, not simply perception. Stacked waveforms (top and bottom) adopt the axes noted on the first waveform. (**B**) At ~320 ms, the LFP pattern suggests inflectional processing. (**C**) At ~450 ms, in a channel 5 mm distant, the complementary pattern suggests phonological processing. (Inset) MRI slices from this patient, annotated with the anatomical location of A4, the contact in common to the two channels reported here. Statistical significance: **** ($P < .0001$), *** ($P < .001$), ** ($P < .01$) (*t* test, one tail, two-sample, equal variance). Box arrows (bottom) indicate linguistic processing stages, which may be interposed among other stages not addressed here.

studies have tied it to a broad variety of linguistic and nonlinguistic processes (*15*). This uncertainty may be a consequence of the coarseness of current measurements. It remains possible that grammatical and other linguistic processes are processed distinctly, even sequentially, in the microcircuitry of the brain, but techniques that sum over seconds and centimeters necessarily blur them.

In a rare procedure, electrodes are implanted in the brains of patients with epilepsy for clinical evaluation. Recordings of intracranial electrophysiology (ICE) from unaffected brain tissue during periods of normal activity can provide millisecond resolution in time with millimeter resolution in space. We recorded local field potentials (LFP) from multicontact depth electrodes in three right-handed patients (ages 38 to 51, with above-average language and cognitive skills) whose electrodes were located in and around Broca's area while they read words verbatim or converted them to an inflected form (past/present or singular/plural) (Figs 1 and 2) (*16*). The task engages inflectional morphology, which is like syntax in combining meaningful elements according to grammatical rules, but the units are shorter and semantically simpler, making fewer demands on working memory and conceptual integration, and thus allowing greater experimental control. We applied the high resolution of ICE to a task that distinguishes three linguistic processes to investigate the spatiotemporal patterning of word production in the brain.

In each trial, participants saw either the instruction "Repeat word" (the "Read" condition) or a cue that dictated an inflected form ("Every day they ____"; "Yesterday they ____"; "That is a ____"; "Those are the ____"). Next, they saw a target word and produced the appropriate form silently (Fig. 1A) (*16*). The 240 target words were presented in uninflected form in the phrase "a [noun]" or "to [verb]" (*17*) (Fig. 1B). Half the targets were regular (e.g., "link"/"linked") and half irregular (e.g., "think"/"thought"), to ensure that participants had to access the word rather than automatically appending the regular suffix (*18*).

The Null-Inflect (N) condition requires an inflected form of the verb (present tense) or noun (singular), yet these forms are not overtly marked and thus require the same output to be pronounced as in the Read (R) condition. The difference between these conditions thus implicates the process of inflection. In contrast, the Overt-Inflect (O) condition (past-tense verb or plural noun) requires that a suffix be added (regular) or the form changed (irregular). It thus differs from the Null-Inflect condition in requiring computation of a different phonological output (Fig. 1B). (The label "phonological" subsumes phonological, phonetic, and articulatory processes.) The design was fully crossed, with trials presented in pseudorandom order.

To assess whether these patients' language systems were organized normally, and to correlate LFP with fMRI, we performed fMRI in two of the patients before their electrodes were placed. Their activation patterns were indeed similar to 18 healthy controls (Fig. 3, A to C) [for other fMRI results, see (*19*)]. Most of the 168 bipolar channels from which we recorded (across patients) were in fMRI-active regions (Fig. 3, A to G). LFP that was significantly correlated with the task ($P < .001$, corrected) [see (*16*)] was recorded in about half (86 of 168) of the channels (19 channels in

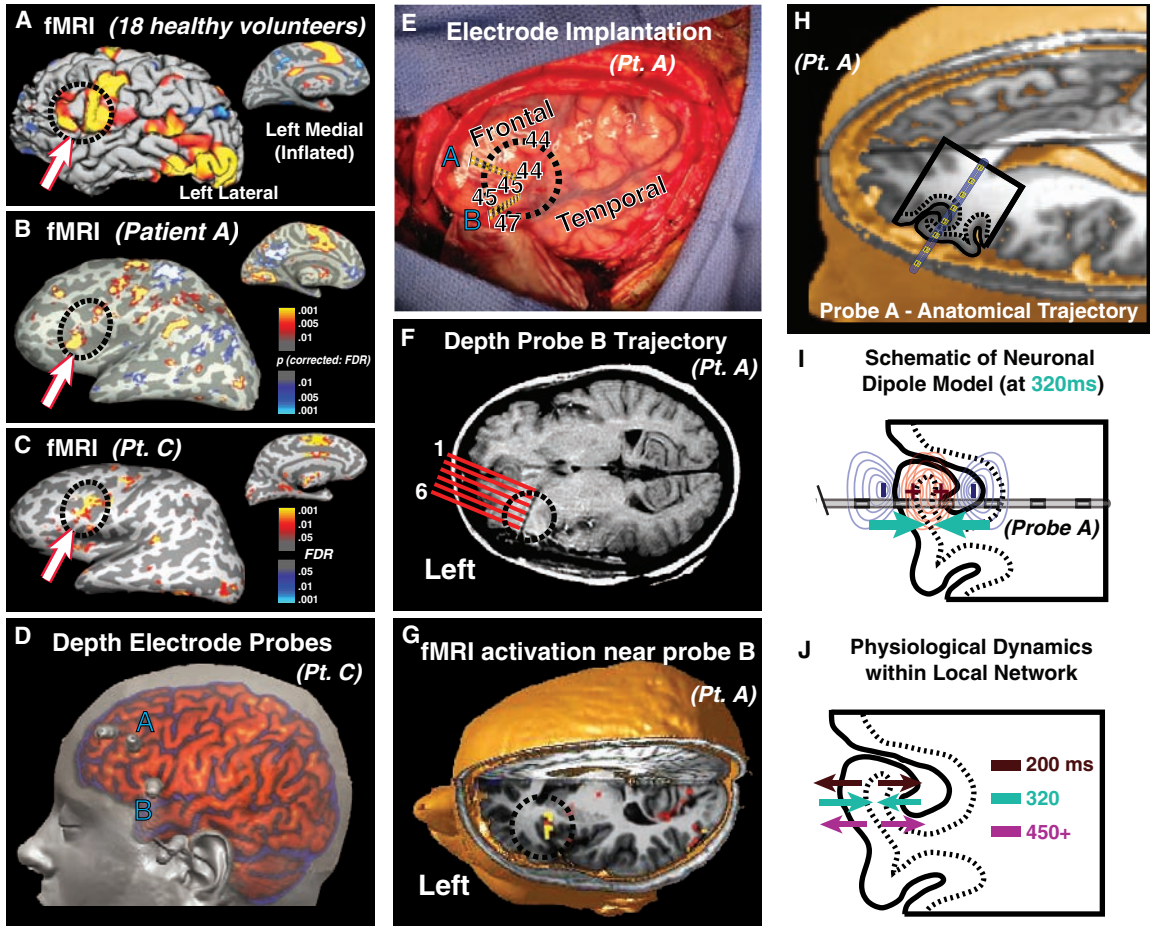

Fig. 3. Localization of fMRI responses, depth electrodes, and neural generators. (**A**) fMRI in 18 controls, contrasting activity for all task conditions with visual-fixation baseline periods. The task engages classic language areas (Broca's, speech-related motor cortex, medial supplementary motor area, anterior cingulate, and superior temporal lobe) and visual-reading areas (visual word form area and primary and ventral visual cortex). Classic Broca's area is circled. Thresholding and correction at a 0.01 false discovery rate (*16*). Scale as in (B). (**B** and **C**) Single-patient fMRI (identical contrast) reveals similar activations in both patients and controls. Surfaces are inflated to reveal activation within sulci. (**D**) Coregistered MRI and computerized tomography scan of patient C showing depth probes inserted through the skull. (**E**) Intra-operative photo showing left perisylvian language areas. Letters, insertion points of the probes; dashed lines, surface projections of their intracortical trajectories. Putative Brodmann areas are labeled. (**F**) Postimplantation MRI reveals that probe B traverses Broca's area in the posteromedial process of IFG pars opercularis facing the insula, and preimplantation fMRI (**G**) demonstrates that the region was activated by the task in this patient. (**H**) Location of probe A, in Broca's area traversing IFG pars triangularis within the inferior frontal sulcus. (**I** and **J**) Schematic of neural dipoles near probe A that generated the LFP components, hypothesized from their polarities, amplitudes, and locations (see fig. S3). Schematic gyral outline corresponds to the gyral trace superimposed on the MRI in (H).

patient A, 37 in B, and 30 in C). Of these channels, 49 (57%) were within Broca's area or the anterior temporal lobes (16 in patient A, 19 in B, 14 in C). Of the 49 channels, 26 were within Broca's area, and the majority (20 of 26) yielded a strong triphasic (three-component) LFP waveform (9 in patient A, 8 in B, 3 in C). The mean peaks occurred ~200, ~320, and ~450 ms after the target word onset (Fig. 2A), and this timing was consistent across patients (Fig. 4, A and B, and figs. S1, S4, and S5).

The three LFP components showed signatures of distinct linguistic processing stages (Fig. 2, A to C). The ~200-ms component appears to reflect lexical identification. The timing converges with when word-specific activity has previously been recorded in the visual word form area (VWFA) [(*20*, *21*), but see (*22*)] and when the VWFA has been shown to become phase-locked with Broca's area (*23*). Furthermore, the magnitude of the component varied with word frequency, which indexes lexical access (*24*). Specifically, rare words (frequency 1 to 4) yielded a significantly higher amplitude [$t(204) = 3.32$, $P < 0.001$] than common words (frequency 9 to 12) (Fig. 2A) (*25*). Word frequency is inversely correlated with word length, but the present effect is not a consequence of length: We found no difference at ~200 ms between short (2 to 4 characters) and long (6 to 11 characters) words (Fig. 2A), nor a difference between one-morpheme and two-morpheme responses (*26*). Later components were not affected by frequency. Finally, consistent with the fact that lexical identification is required by all three inflectional conditions, the ~200-ms component did not vary across them. Primary lexical access is generally associated with temporal cortex rather than Broca's area (*8*), so this component may index delivery of word identity information into Broca's area for subsequent processing, consistent with anatomic and physiological evidence that the two areas are integrated (*23*, *27*). Although word-evoked activity in this latency range has previously been localized to Broca's area with LFP (*28*) and magnetoencephalography (*29*), it has not been demonstrated to be modulated by lexical frequency.

The subsequent two LFP components showed activity patterns predicted for grammatical and phonological processing, respectively (Fig. 2, B and C). In the ~320-ms component (Fig. 2B), the Overt-Inflect and Null-Inflect conditions significantly differed from the Read condition but not from each other. Thus, the ~320-ms component is modulated by the demands of inflection (required by Overt-Inflect and Null-Inflect but not Read), but not by the demands of phonological programming (required in Overt-Inflect but not in Null-Inflect or Read; see Fig. 1C). In contrast, in a component appearing at ~450 ms, Overt-Inflect did differ from the Null-Inflect and Read conditions, which did not differ from each other (Fig. 2C). This contrasting pattern indicates that the ~450-ms component reflects phonological, phonetic, and articulatory programming, independently confirmed by its sensitivity to the number of syllables (Fig. 4C). Both components were recorded from Broca's area in all patients (fig. S1), and specifically in patient A (Fig. 2) from the inferior frontal gyrus (IFG) pars triangularis deep in the inferior frontal sulcus. The ~320-ms component was recorded near the fundus; the ~450-ms component was recorded 5 mm more lateral along the sulcus within a subgyral fold that faced the fundus (Fig. 3I and fig. S1A). This region is often considered part of area 45 [but see (*30*)].

The pattern of sign inversions across neighboring bipolar channels in space (Fig. 2A, top) indicates that the generators of the LFP components were local (fig. S3), and the differences in inversions across components in time indicate that their generators were not identical (Fig. 3, I and J). Thus, the overall LFP pattern suggests a fine-grain spatiotemporal progression of lexical, grammatical, and phonological processing within Broca's area during word production.

The triphasic pattern in all patients was found exclusively in Broca's area (Fig. 4A). Outside Broca's area, other patterns prevailed; for example, temporal lobe sites showed a slow and late monophasic component at 500 to 600 ms (Fig. 4A, bottom, and fig. S4, F and G) (*31*), possibly reflecting self-monitoring (*7*, *8*). The condition differences for each component were also consistent across patients, replicating the temporal isolation of grammatical (~320 ms) from phonological (~450 ms) processing (fig. S1). The word-frequency effect on the ~200-ms component was significant in patients A and B and marginal ($P = 0.06$) in patient C (fig. S2). The ~200-, ~320-, and ~450-ms components were consistent in their timing across patients, although the keypress reaction times, which require the self-monitoring process, varied among patients and conditions (fig. S6).

Although nouns and verbs differ linguistically and neurobiologically (*32*, *33*), the neuronal activity they evoked was similar (Fig. 4B). Furthermore, the patterning across inflectional conditions was the same for nouns and verbs (*34*). These parallels suggest that words from different lexical classes feed a common process for inflection.

Additional evidence that the LFP patterns reflect inflectional computation is that they are triggered by presentation of the target word, not the cue, even though the cues contain more visual and linguistic elements (Fig. 4D) (*35*). Furthermore, activity evoked by the cue showed little sensitivity to the inflectional conditions.

The LFP patterns are consistent with the computational nature of the task and with independent estimates of the timing of its subprocesses. Inflectional processing cannot occur before the word

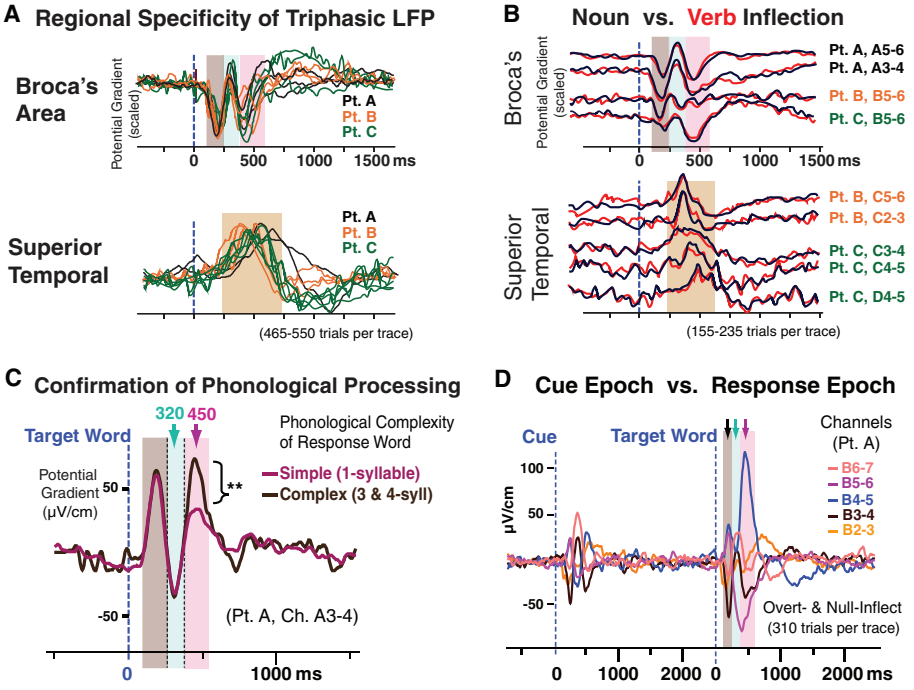

Fig. 4. Additional features of the triphasic waveform support the lexical-inflectional-phonological progression. (**A**) Triphasic activity is specific to Broca's area and is consistent across patients. All-condition average waveforms from task-active channels in each patient are superimposed (scaled in amplitude to a single channel in each region and standardized in polarity). (**B**) Noun (black) and verb (red) inflection (Null and Overt combined) involved nearly identical neural activity, across sites and patients. Standardized across channels in polarity. (**C**) The ~450-ms component, which is sensitive to phonological differences among inflectional conditions, is also sensitive to phonological complexity (syllable count) of the target word ($P < 0.01$, corrected). (**D**) Neural activity in Broca's area is evoked primarily when processing the target word (when the linguistic processing of interest should occur), not the cue (*35*).

is identified (especially as to whether it is regular or irregular), and phonological, phonetic, and articulatory processing cannot be computed before the phonemes of the inflected form have been determined. Word identification has been shown to occur at 170 to 250 ms (*8*, *29*, *36*), consistent with the ~200-ms component, and syllabification and other phonological processes at 400 to 600 ms, consistent with the phonological component at 400 to 500 ms (*8*). In naming tasks, speech onset occurs at around 600 ms (*8*), which is consistent with the self-monitoring behavioral responses we recorded (fig. S6). Self-monitoring has been localized to the temporal lobe (*8*), where we recorded LFPs in the post-response latency range that may correspond to previously described scalp event-related potentials (*37*). Working backward from 600 ms, we note that motor neuron commands occur 50 to 100 ms before speech, placing them just after the phonological component we found to peak at 400 to 500 ms (*38*). In sum, the location, behavioral correlates, and timing of the components of neuronal activity in Broca's area suggest that they embody, respectively, lexical identification (~200 ms), grammatical inflection (~320 ms), and phonological processing (~450 ms) in the production of nouns and verbs alike.

Although the language processing stream as a whole surely exhibits parallelism, feedback, and interactivity, the current results support parsimony-based models such as LRM (*7*), in which one portion of this stream consists of spatiotemporally distinct processes corresponding to levels of linguistic computation. Among the processes identified by these higher-resolution data is grammatical computation, which has been elusive in previous, coarser-grained investigations. As such, the results are also consistent with recent proposals that Broca's area is not dedicated to a single kind of linguistic representation but is differentiated into adjacent but distinct circuits that process phonological, grammatical, and lexical information (*37*, *39*–*41*).

References and Notes

1. S. Pinker, *The Language Instinct* (HarperColllins, 1994).
2. S. Pinker, *Science* **253**, 530 (1991).
3. K. Plunkett, V. Marchman, *Cognition* **38**, 43 (1991).
4. B. MacWhinney, J. Leinbach, *Cognition* **40**, 121 (1991).
5. M. F. Joanisse, M. S. Seidenberg, *Proc. Natl. Acad. Sci. U.S.A.* **96**, 7592 (1999).
6. J. L. McClelland, *Psychol. Rev.* **86**, 287 (1979).
7. W. J. M. Levelt, A. Roelofs, A. S. Meyer, *Behav. Brain Sci.* **22**, 1 (1999).
8. P. Indefrey, W. J. M. Levelt, *Cognition* **92**, 101 (2004).
9. D. P. Janssen, A. Roelofs, W. J. M. Levelt, *Lang. Cogn. Process.* **17**, 209 (2002).
10. N. Dronkers, *Nature* **384**, 159 (1996).
11. We use "Broca's area" to denote the left IFG pars opercularis and pars triangularis [classically, Brodmann areas 44 and 45, but see (*30*)].
12. P. Broca, *Bulletin de la Société Anatomique* **6**, 330 (1861).
13. E. Zurif, A. Caramazza, R. Myerson, *Neuropsychologia* **10**, 405 (1972).
14. Y. Grodzinsky, *Behav. Brain Sci.* **23**, 1 (2000).
15. E. Kaan, T. Y. Swaab, *Trends Cogn. Sci.* **6**, 350 (2002).
16. Materials and methods are available as supporting material on *Science* Online.
17. The context words ("a" and "to") prevented participants from simply concatenating the cue and target (a strategy that would succeed in two-thirds of the trials) and helped equalize difficulty across conditions.
18. Differences in the signals between regular and irregular verbs are not analyzed here [for discussion, see (*19*)].
19. N. T. Sahin, S. Pinker, E. Halgren, *Cortex* **42**, 540 (2006).
20. L. Cohen, S. Dehaene, *Neuroimage* **22**, 466 (2004).
21. A. C. Nobre, T. Allison, G. McCarthy, *Nature* **372**, 260 (1994).
22. C. J. Price, J. T. Devlin, *Neuroimage* **19**, 473 (2003).
23. N. T. Sahin *et al.*, *Neuroimage* **36**, S74 (2007).
24. O. Hauk, F. Pulvermuller, *Clin. Neurophysiol.* **115**, 1090 (2004).
25. Frequency score was the rounded natural log of the combined frequencies of all inflectional forms of a word, plus one.
26. These factors were largely independent. Word length correlated little with morpheme count (0.267) or frequency (–0.347).
27. A. D. Friederici, *Trends Cogn. Sci.* **13**, 175 (2009).
28. E. Halgren *et al.*, *J. Physiol. (Paris)* **88**, 51 (1994).
29. K. Marinkovic *et al.*, *Neuron* **38**, 487 (2003).
30. K. Amunts *et al.*, *J. Comp. Neurol.* **412**, 319 (1999).
31. This component may approximate the P600 component often recorded from the scalp (*42*), but comparisons are difficult because the P600 is generally elicited by errors, in comprehension rather than production experiments.
32. A. Caramazza, A. E. Hillis, *Nature* **349**, 788 (1991).
33. K. Shapiro, A. Caramazza, *Trends Cogn. Sci.* **7**, 201 (2003).
34. The exception was that, for nouns, the Overt-Read comparison at ~320 and the Overt-Null comparison at ~450 ms only approached significance ($P = 0.08$ and 0.06, respectively; one-tailed t test).
35. We measured the average amplitude of the rectified all-conditions LFP in Broca's area channels in all patients, in the 150- to 650-ms interval, embracing our components of interest. The response epoch had a higher amplitude than the cue epoch in most (20 of 26) channels, and across all channels was 99% greater. [Patient A yielded a higher amplitude in the response epoch in 7 of 10 channels, on average 71.7% higher; patient B in 7 of 10 channels (+33.6% on average); and patient C in 6 of 6 channels (+191.6% on average)].
36. R. Gaillard *et al.*, *Neuron* **50**, 191 (2006).
37. A. D. Friederici, *Trends Cogn. Sci.* **6**, 78 (2002).
38. LFP components reported here vary by amplitude but not latency or duration; evidently, the processes they index are consistently timed, and other processes [e.g., assembly and enactment of the articulatory plan (*8*)] produce the differences in response latency.
39. P. Hagoort, *Trends Cogn. Sci.* **9**, 416 (2005).
40. I. Bornkessel, M. Schlesewsky, *Psychol. Rev.* **113**, 787 (2006).
41. However, the fine-grained, within-gyrus localization reported here cannot easily be mapped onto the more macroscopic divisions suggested by these authors.
42. A. D. Friederici, *Clin. Neurosci.* **4**, 64 (1997).

43. Supported by NIH grants NS18741 (E.H.), NS44623 (E.H.), HD18381 (S.P.), T32-MH070328 (N.T.S.), NCRR P41-RR14075; and the Mental Illness and Neuroscience Discovery (MIND) Institute (N.T.S.), Sackler Scholars Programme in Psychobiology (N.T.S.), and Harvard Mind/Brain/Behavior Initiative (N.T.S.). We heartily thank the patients. We also thank E. Papavassiliou and J. Wu for access to their patients; S. Narayanan, N. Dehghani, M. T. Wheeler, F. Kampmann, and L. Gruber for assistance with intracranial electrophysiological data; R. Raizada for manuscript suggestions; N. M. Sahin; and two anonymous reviewers whose suggestions and encouragement greatly improved this paper.

Supporting Online Material

www.sciencemag.org/cgi/content/full/326/5951/445/DC1
Materials and Methods
Figs. S1 to S6
Tables S1 and S2
References

3 April 2009; accepted 28 August 2009
10.1126/science.1174481

Fast Synaptic Subcortical Control of Hippocampal Circuits

Viktor Varga,[1*†] Attila Losonczy,[2*†‡] Boris V. Zemelman,[2*] Zsolt Borhegyi,[1] Gábor Nyiri,[1] Andor Domonkos,[1] Balázs Hangya,[1] Noémi Holderith,[1] Jeffrey C. Magee,[2] Tamás F. Freund[1]

Cortical information processing is under state-dependent control of subcortical neuromodulatory systems. Although this modulatory effect is thought to be mediated mainly by slow nonsynaptic metabotropic receptors, other mechanisms, such as direct synaptic transmission, are possible. Yet, it is currently unknown if any such form of subcortical control exists. Here, we present direct evidence of a strong, spatiotemporally precise excitatory input from an ascending neuromodulatory center. Selective stimulation of serotonergic median raphe neurons produced a rapid activation of hippocampal interneurons. At the network level, this subcortical drive was manifested as a pattern of effective disynaptic GABAergic inhibition that spread throughout the circuit. This form of subcortical network regulation should be incorporated into current concepts of normal and pathological cortical function.

Subcortical monoaminergic systems are thought to modulate target cortical networks on a slow time scale of hundreds of milliseconds to seconds corresponding to the duration of metabotropic receptor signaling (*1*). Among these ascending systems, the serotonergic raphe-hippocampal (RH) pathway that primarily originates within the midbrain median raphe nucleus (MnR) is a key modulator of hippocampal mnemonic functions (*2*). Contrary to the slow modulatory effect commonly associated with ascending systems, electrical stimulation of the RH pathway produces a rapid and robust modulation of hippocampal electroencephalographic activity (*3*–*5*). Anatomical evidence shows that MnR projections form some classical synapses onto GABAergic interneurons (INs) in the hippocampus (*6*), potentially providing a substrate for a fast neuromodulation of the hippocampal circuit. Recent reports of the presence of glutamate

Supporting Online Material – Sahin, *et al.*

"Sequential Processing of Lexical, Grammatical, and Phonological Information within Broca's Area"
Ned T. Sahin, Steven Pinker, Sydney S. Cash, Don Schomer, Eric Halgren
SCIENCE, vol. 326, no. 5951, pp. 445-449 (Oct 16, 2009).

Materials and Methods

Patients and Testing

Patients had a history of complex partial seizures, and were under care at the Beth Israel Deaconess Medical Center (BIDMC). They were candidates for elective surgical treatment because their seizures did not respond to medications or other less-invasive treatments, and the source of their epilepsy was thought to be focal and located in an operable brain region. Depth electrode probes were implanted in each patient's brain in order to localize the seizure focus and thus direct surgical treatment (Fig. 3). Clinical decisions such as whether, where and for how long to implant electrodes for presurgical diagnosis were made purely for clinical reasons, and independently of this study. Patients gave written informed consent according to NIH guidelines as monitored by the BIDMC institutional review board (IRB).

Patients were selected for inclusion in the present study according to restrictive criteria: well-above-average overall cognitive and language abilities, no clinical language impairments, native English language competence, right-handedness; and electrode placement that included the traditional language regions hypothesized to be engaged by our task. Seizure foci were clinically determined to lie outside the regions from which data are reported (classic language areas and medial temporal lobes). The selection factors were designed to ensure that patients had relatively normal language development, and were corroborated by running the same task with fMRI and comparing their data to normal controls (Fig. 3). Patients performed the task first in fMRI, and then 4-16 days after electrodes had been implanted (Table S1).

Patient	Sex	Age	Seizure Onset Age	fMRI Performed?	Testing Day	Completed Runs (of 9)
A	F	41	14	Yes	13	6
B	F	51	18	No	16	9
C	F	38	5	Yes	4	7

Table S1. Patient information. Patient B first experienced loss of consciousness at age 18, but in retrospect the family reported intermittent spells at age 4.

During testing, patients were alert and focused, and their hospital room doors were kept closed, with no interventions by clinical staff. Stimuli were presented on a laptop computer positioned at a comfortable height, 0.5–1.0 m from the patient's eyes. Patients pressed the space bar with their left hand when a keypress was required.

Electrodes

Depth probes were SD08R–SP10X–000 eight-contact depths from Ad-Tech® Medical Instrument Corporation, 1.0 mm in diameter with eight contacts spaced 5 mm from center to center. The probes were inserted through the lateral cortical surface, providing a linear array of electrode contacts able to record from the gray matter structures through or near which they passed. Recordings were obtained from successive pairs of contacts, each subtracted from the next (Fig. 2A), creating seven bipolar (differential) recording channels per probe. Differential recordings are less noisy and more focal than monopolar.

The Broca's area contacts were available for the present research because they lay on the trajectory of probes that targeted more medial regions (anterior cingulate or orbitofrontal cortex), which prior non-invasive clinical monitoring revealed were among the areas where seizures might have arisen. In addition, the contacts in or near Broca's area helped the clinical team determine how far the epileptogenic zones penetrated into eloquent cortex, allowing them to plan a resection providing maximum seizure relief with minimal neuropsychological consequences.

The number of electrode contacts across all patients which functioned normally was 168. Some electrodes that were implanted malfunctioned and produced no usable data; these were not analyzed nor considered in the counts reported here. The precise anatomical location of each electrode contact was determined with MRI and/or CT scans taken with the electrodes in place, in conjunction with pre-implantation MRI when useful. All analyses are based on this direct and unambiguous localization. Separately, in order to provide standardized coordinates to compare with other studies, we manually transformed each patient's brain according to the Talairach standard brain (*S1*) to determine coordinates similar to MNI coordinates. The three-dimensional origin (0,0,0 point) was set as the posterior-superior aspect of the anterior commissure at midline. The x,y,z coordinate in millimeters (normalized) are reported for the contacts of greatest interest, after piecewise linear normalization to the Talairach brain (Table S2).

Intracranial Analysis

Continuous intracranial electroencephalography (iEEG) was collected, along with timing pulses (triggers) sent from the stimulus presentation program (Presentation™ by Neurobehavioral Systems) to signal the onset of each trial of the task. Data were band-pass filtered from 0.1 to 100 Hz; and digitized at 200 Hz (Patient A) or 800 Hz (Patients B, C). Depth iEEG provides the spatial distribution of local field potentials (LFP), which directly correspond to excitatory, inhibitory, and active transmembrane currents.

Analysis was performed with Neuroscan SCAN 4.3.3 software from Compumedics, and software created by one of the authors (N.T.S.) to automate analysis and perform advanced visualization. Time periods that included gross motion artifacts (roughly 2% of the trials) were excluded from further analysis by a trained operator. Data were band-pass filtered with a zero-phaseshift FIR filter (48 dB/oct) between 0.5 Hz and 40Hz (20 Hz for Patient C). The high-pass cutoff was 1.5 Hz in Patient B to remove very slow components, which were not modulated by the task conditions. Continuous data were epoched based on the stimulus presentation time as recorded in the experiment log files. Epoched data were baseline-corrected based on the pre-stimulus intervals for each channel. Filtering and epoching were accomplished using the built-in functions within Neuroscan SCAN 4.3.3 software.

Averages were computed as the point-by-point voltage deviation from a mean voltage value (normalized to zero) recorded by the given channel during a baseline period (the 750 ms before the stimulus onset), averaged over all trials of the given experimental condition. Averaged waveforms yielded the task-locked or evoked signal, and thus constituted intracranial event-related potentials (iERPs) or task-evoked LFP for the given condition.

Statistics

Our statistical strategy was to: (1) identify all recording channels in or near Broca's area; (2) select those channels with significant overall task-related activity; (3) select significant iERP components in these channels; and (4) apply three planned comparisons (Fig. 1) to characterize the linguistic computation represented by the components.

Channels that recorded from Broca's area were identified by inspecting structural MRIs, which were acquired for clinical purposes with the probes in place. To select channels with significant task-related activity, we first identified the maximum voltage in the all-condition average waveform for each channel. We then analyzed the signal trial by trial, at the time point of that maximum, using a one-tailed *t*-test (two-sample, equal variance) to compare the task trials to baseline periods interspersed among trials (the Fixation condition). If the peak differed significantly from the baseline activity (tested at $P < 0.001$, corrected for multiple comparisons), the channel was included for further analysis. Bonferroni correction was based on the total number of channels in Broca's region across patients (45). These criteria resulted in 26 of these channels being designated as active.

Visual inspection revealed that most Broca's area channels recorded three iERP components, falling in three discrete time windows (see Fig. 2, Fig. 4, fig. S1, fig. S3, fig. S4, fig. S5). Within each task-active channel, components meeting a test for significance at $p<0.001$ (corrected) were selected for further analysis (one-tailed *t*-test, two-sample, equal variance). Some components were as significant as $p<10^{-150}$ (fig. S5). Bonferroni correction was based on the number of channels selected as above multiplied by three (the number of time windows), for a total correction factor of 78. We then applied planned comparisons among inflectional conditions (see Fig. 1B and C) within each selected component as trial-by-trial one-tailed *t*-tests (two-sample, equal variance).

For one analysis, we further divided each condition by word class: nouns versus verbs. The lower signal-to-noise ratio due to fewer trials in each condition was mitigated by comparing the average voltage during a time window of +/- 30 ms around the peak for each trial rather than the instantaneous voltage at the peak. The peak latency was derived from the average waveform across all inflectional conditions (but separately for noun trials or verb trials respectively).

A separate analysis was performed to determine if the reported effects could also be observed in modulation of gamma power. Power in two bands was examined, low-gamma (25-55 Hz) and high-gamma (70-100 Hz), for channels and latencies where LFP differences by inflectional condition are reported. Spectral power was calculated using Morlet wavelets in each trial individually and then averaged across trials. Although gamma power was modulated relative to baseline, no significant differences were found between task conditions.

fMRI Recording and Analysis

fMRI data were collected with a Siemens Magnetom Trio 3-Tesla whole-body system with a Siemens head coil. BOLD contrast was obtained with a gradient-echo echo-planar imaging (EPI) sequence, TR = 2.6 sec; TE = 30 ms; flip angle = 90; FOV = 200 mm; base matrix = 64 x 64 (3.125 x 3.125 mm in-plane resolution). For each volume, 36 axial 3.0 mm slices (parallel to the AC–PC plane) were collected to cover the brain. High-resolution structural images were collected with a three-dimensional MPRAGE protocol, at 1.0 x 1.0 x 1.33 mm resolution.

fMRI data were analyzed using the FreeSurfer and FS–FAST software packages from the Massachusetts General Hospital Athinoula A. Martinos Center for Biomedical Imaging, and Cortechs Labs, LLC (La Jolla, CA). Automation of the fMRI analysis and visualization were performed by custom software created by one of the authors (N.T.S.). fMRI from the group of 18 healthy volunteers was analyzed as described previously (*S2*), although the contrast reported here (Fig. 3A) was not previously reported. The present contrast results were normalized to, and displayed upon, the cortical surface of Patient A.

The T1-weighted structural images were processed through FreeSurfer to reconstruct the cortical surface (*S3*, *S4*). The surface was then registered with a surface-based atlas (*S5*). Functional (EPI) data were motion-corrected using AFNI (*S6*), spatially smoothed with a 7 mm FWHM Gaussian kernel, and intensity-normalized (over time and space) to a grand mean value of 1000. The functional volume was registered to the structural (T1) volume in order to align the activation maps with the cortical surface. The hemodynamic response function (HRF) was modeled using a gamma-variant function with a delay of 2.25 sec and a dispersion of 1.25 sec (*S7*). The HRF amplitude for each event type was estimated at each voxel using a general linear model (GLM). Autocorrelation in the fMRI noise was accounted for by pre-whitening with a filter estimated from the residual autocorrelation function averaged over all brain voxels (*S8*). Low-frequency drift was removed by including a fifth-order polynomial in the GLM. Contrasts were computed as linear combinations of the HRF amplitudes (i.e., regression coefficients).

Correction for multiple comparisons was carried out using the False Discovery Rate (FDR) technique (*S9*). A global region-of-interest (ROI) was selected to include all voxels that were significant at the .001 level (voxel-wise) in an omnibus contrast (i.e., all tasks versus fixation). The voxel-wise corrected threshold for each contrast-of-interest (COI) was chosen to achieve an FDR of .01 within all voxels of the global ROI for data included in that COI. This means that no more than 1% of the voxels ruled "active" in each contrast were in fact noise (5% for Patient C in Fig. 3C). Note that constraining the ROI based on the omnibus activation does not bias the findings for the COIs; that is, it does not make it more or less easy to find false positives for a given COI, since the data for the COI are compared against all voxels active in the experiment. Similarly, the significance threshold used to select the global ROI does not bias the findings for the COIs.

Behavioral Task & Behavioral Data

Subjects produced a grammatically inflected word in response to a visually-presented target word, or simply read back the target word. Each target word was preceded by a brief frame that signaled the inflectional condition and thus the expected response. Frames were short incomplete sentences or instructions (Fig. 1B). Subjects produced the response silently: they were instructed to think the word, concentrate on the mental utterance and avoid other distracting thoughts. They were further instructed to press a keyboard button after completing the silent utterance. For example, a patient who saw "Yesterday they___." then "to walk" would subvocally produce "walked", then press the button. The full set of 240 words was presented across three runs of approximately 6 minutes each, and the sets of runs were repeated once or twice in varying orders.

The task required a minimum of semantic processing and thus varied little among conditions. Furthermore, the grammatical manipulation did not involve movement or other filler-gap dependencies and thus imposed minimal demands on short-term linguistic memory. A virtual "Fixation" condition comprised epochs inserted pseudo-randomly to jitter the task trials in time. Patients visually fixated on the "x" in the center of the screen. This was used as a low baseline for event-related fMRI and iEEG analysis.

There was no direct measure of reaction time or performance accuracy in this task, because participants responded covertly (silently) to avoid auditory feedback, and to afford maximal compatibility with the fMRI procedure, where silent responses were used to avoid jaw and head movements. The key-press task was there mainly to ensure that Patients complied with the task; the reaction-time data they provide is approximate and indirect because it incorporates variation in patients' monitoring their own task completion time. Patients were aware that the keypresses were not used to cue the trial onset or to evaluate speed or accuracy. Key-press latencies were calculated as the time between the visual onset of the target word and the key-press. Only key-presses that fell after the onset of the word and before the end of the trial (1750 ms) were considered. Latencies were separately considered for each inflectional condition, and a *t*-test (one-tailed, two-sample, equal variance) was performed for each set of conditions within each patient's data (fig. S6).

Supporting Figures

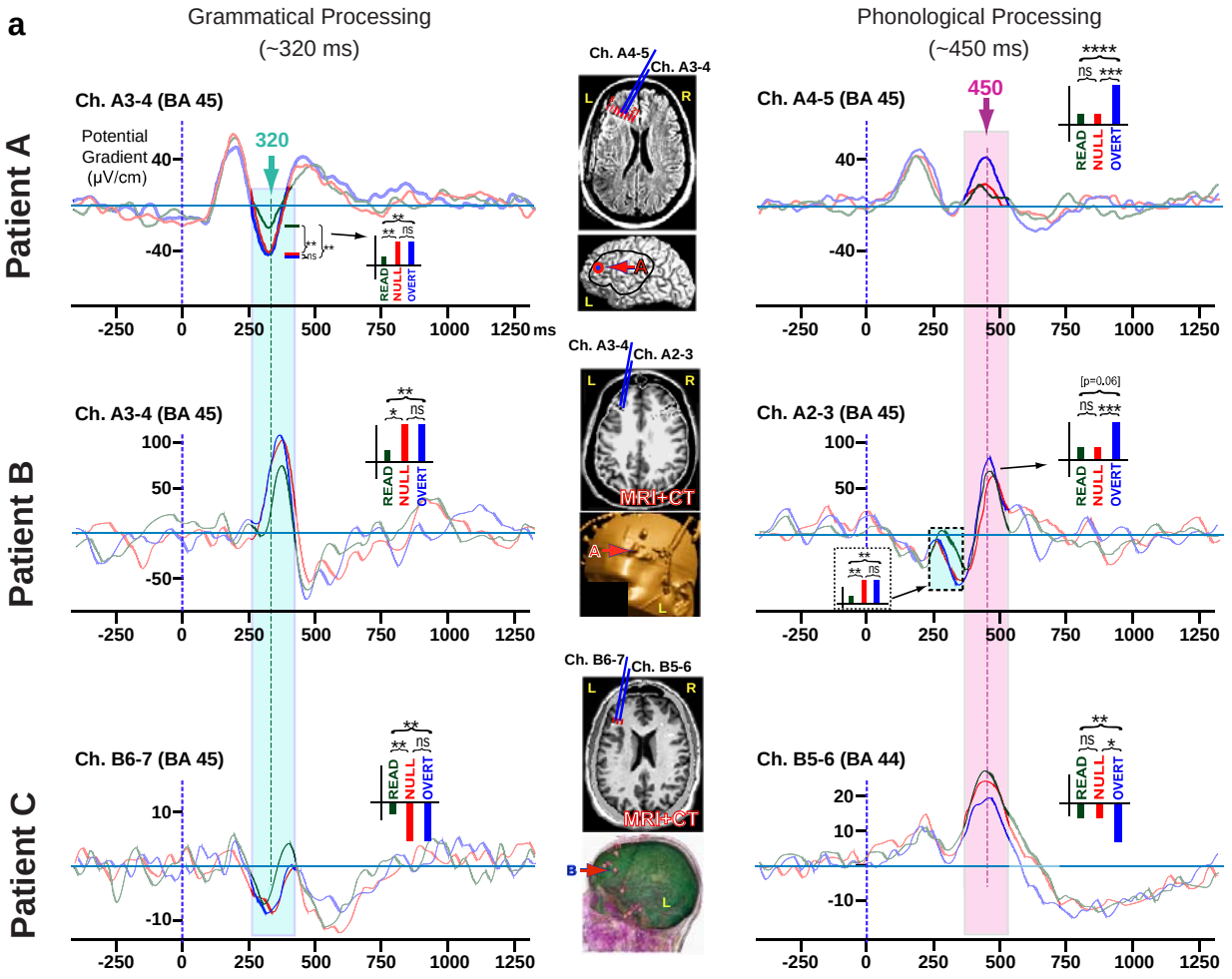

b

Grammatical Processing (~320 ms)

	Channel	Contrast	DF	Time (ms)	T-Score	P-Value	Signif
Patient A	A3-4	Overt-Read	313	335	2.54	0.0059	**
		Overt-Null	304	320	0.01	0.50	ns
		Null-Read	309	320	2.72	0.0035	**
Patient B	A3-4	Overt-Read	468	330	2.51	0.0062	**
		Overt-Null	467	330	0.43	0.33	ns
		Null-Read	467	325	2.14	0.017	*
Patient C	B6-7	Overt-Read	358	355	2.51	0.0062	**
		Overt-Null	358	355	0.00	0.50	ns
		Null-Read	358	355	2.55	0.0056	**

Phonological Processing (~450 ms)

	Channel	Contrast	DF	Time (ms)	T-Score	P-Value	Signif
Patient A	A4-5	Overt-Read	313	465	3.79	0.000090	****
		Overt-Null	304	455	3.12	0.00099	***
		Null-Read	309	455	0.92	0.18	ns
Patient B	A2-3	Overt-Read	468	425	1.53	0.064	[p=.06]
		Overt-Null	467	425	3.11	0.00098	***
		Null-Read	467	450	0.74	0.23	ns
Patient C	B5-6	Overt-Read	361	450	2.46	0.0073	**
		Overt-Null	370	425	2.18	0.015	*
		Null-Read	367	450	0.90	0.18	ns
Patient B	A2-3	Overt-Read	468	330	3.03	0.0013	**
		Overt-Null	467	330	0.93	0.18	ns
		Null-Read	467	330	1.91	0.028	**

fig. S1. Replication across all patients. The existence, timing, temporal isolation, and location in Broca's area of the grammatical and phonological processing components were replicated in all 3 patients. (**a**) For each patient, the average neuronal population response (LFP) for each inflectional condition of the task is plotted and statistically compared according to the planned comparisons for two neighboring recording sites. In the left column the component at ~320 ms in each patient displays the pattern predicted for grammatical processing. In the right column, the component at ~450 ms displays the pattern predicted for phonological processing. In the middle column, the location of each recording channel is displayed within the cortical anatomy of the respective patient. Results of planned comparisons are schematized in the context of histograms signifying the relations in amplitude among the conditions. Statistical significance: **** ($P < 0.0001$), *** ($P < 0.001$), ** ($P < 0.01$) (*t*-test: one tail, two-sample, equal variance). In Patient B, both components were recorded in the same channel. (**b**) Detailed results of the planned comparisons; color-coding and statistical notations as in (a).

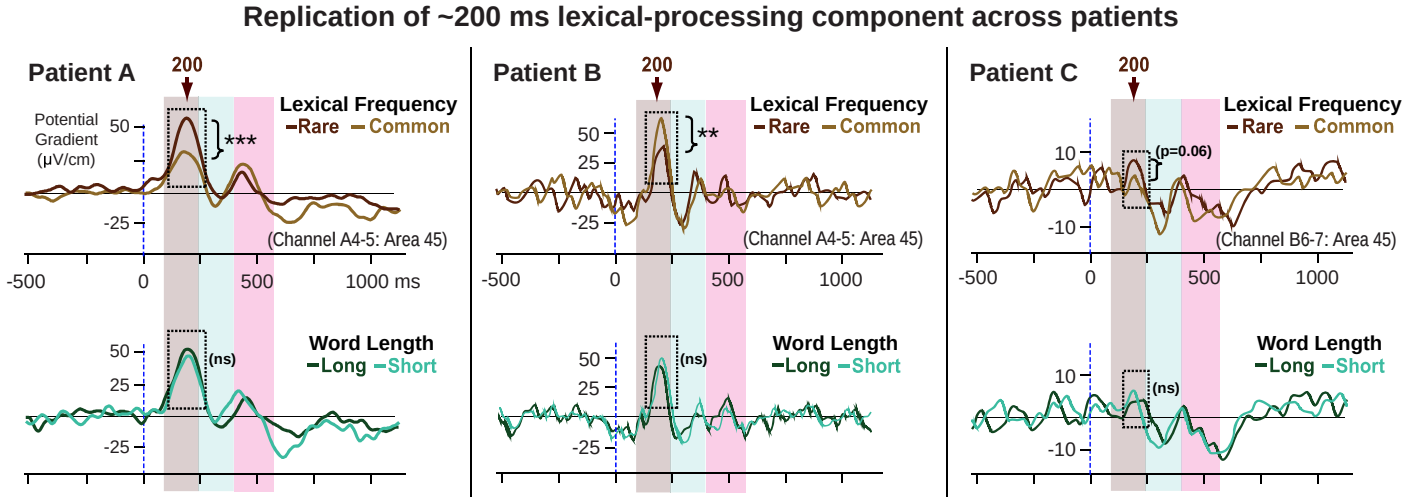

fig. S2. Replication of the ~200 ms lexical component in Broca's area across patients: the component is sensitive to lexical frequency, but not word length. For each patient, trials were sorted and averaged according to the lexical frequency (top) or letterwise length (bottom) of the word presented. See Fig. 1 in the main text for details. In the time window of interest there was no significant effect of word length, indicating that this early component was not driven by this perceptual and low-level feature of the words. Instead, the component was modulated by the lexical frequency of the word (how commonly or rarely it appears in standard corpora; see Methods). This indicates that the component relates to features of the word as a whole, which can only be accessed after the lexical identity of the word has been accessed at least in part. The effect was marginally significant in Patient C ($P = 0.06$ at 208 ms). Statistical significance: *** ($P < 0.001$), ** ($P < 0.01$) (*t*-test: one tail, two-sample, equal variance; point-by-point). All recordings were from Broca's area, in the IFG *pars triangularis*.

Neuronal generators underlying the ~320 ms grammatical processing iERP in dorsal Broca's area

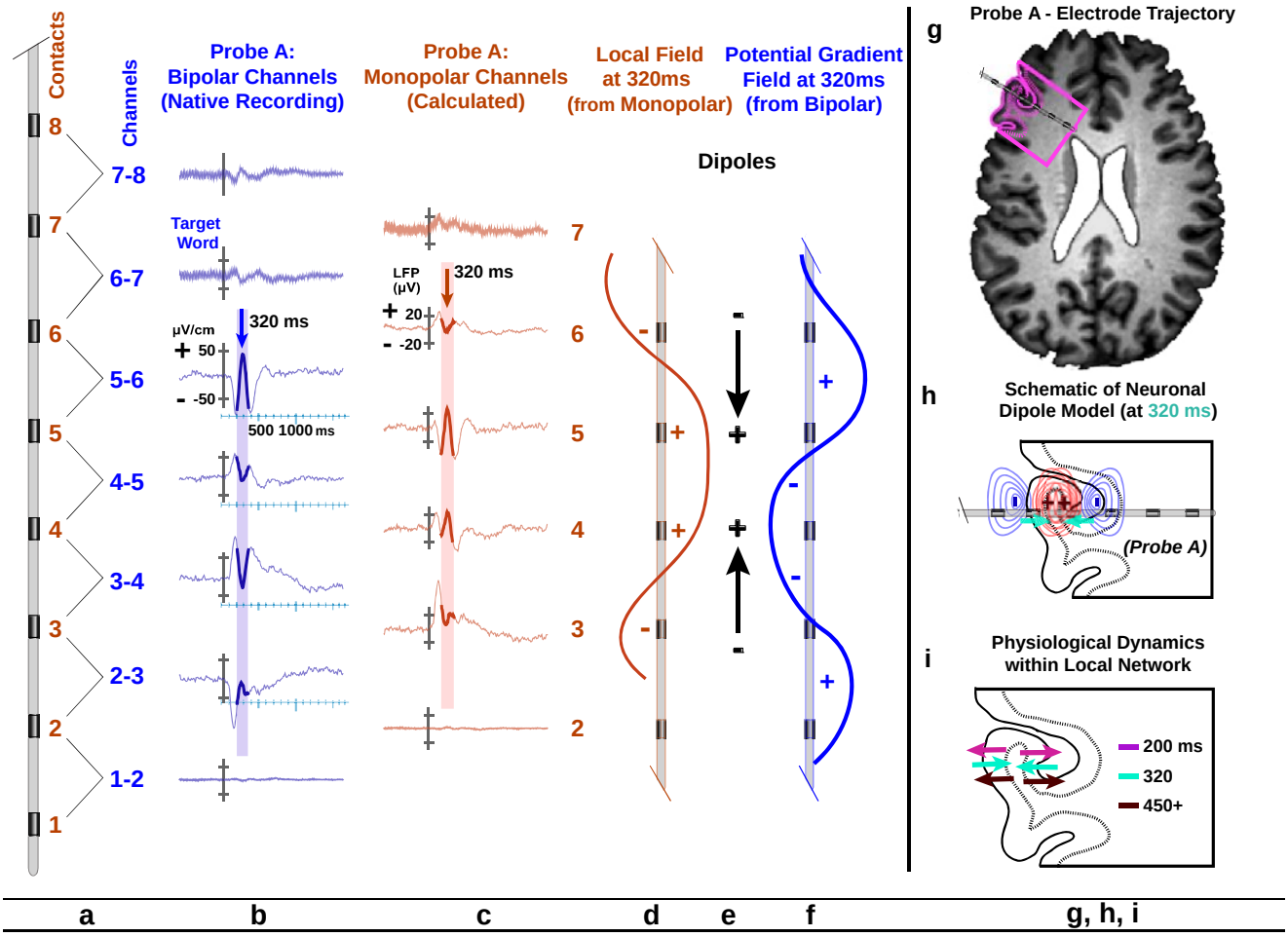

fig. S3. Deducing physiological dynamics. (**a**) Schematic of a depth probe. Numbers denote electrode contacts (orange) and bipolar recording channels (blue). (**b**) Bipolar task-evoked iERPs for each channel on Probe A in Patient A. End channels were outside cortical gray matter and recorded little signal. (**c**) Monopolar iERPs, estimated by re-referencing the bipolar channels on each probe to a common reference channel on the same probe. For instance, bipolar channels A4–5, A3–4, A2–3, and A1–2 were multiplied by –1 and summed, yielding a re-referenced A5–1 bipolar channel. This approximated a monopolar channel A5 because contact A1 was far enough from active generators that local voltage gradients were small, as indicated by the flat average waveforms in channel A1–2. (**d**) Monopolar waveforms were sampled within a narrow time window (~320 +/- 25 ms), to estimate the actual voltage field along the probe axis at the time of the grammatical-processing component. Although the potentials thus recovered may differ by a small amount from the ones that would have been measured had a distant reference been available, that difference would be a constant, and thus these field maps may be used to relate the probe location to the generating dipoles, when considered in concert with the bipolar fields. (**f**) Bipolar waveforms were sampled within the same time window, in order to plot the potential gradient or first spatial derivative of the voltage field (LFP) along the probe. (**e**) Inferred dipoles most consistent with both field lines. (**g**) Anatomical location of Probe A, based on MRI scans. (**h**) Model of the neuronal generator of the ~320 ms iERP component, deduced from the inferred dipoles and the MRI evidence. The probe is inferred to traverse a broadly activated gyrus, recording from both sides, thus yielding the double spatial inversion observed across the central channels. The lack of physiological signal in contacts 1 and 2 results from their location deep in white matter. Similarly, the lack of signal in contacts 7 and 8 results from their location outside the cortex, likely in CSF and skull respectively. (**i**) Model of the generators of the major iERP components.

	Contact	*X* Coordinate (Left to Right)	*Y* Coordinate (Posterior to Anterior)	*Z* Coordinate (Ventral to Dorsal)	Anatomical Location (Direct Localization from Patient's MRI Scan)
Pt. A	A3	-24	29	22	IFG *pars triangularis*, gray matter at fundus of inferior frontal sulcus; BA45
	A4	-28	32	22	IFG *pars triangularis*, gray matter of inner (medial) wall of sub-gyral fold facing the fundus and contact A3; BA45
	A5	-34	34	22	IFG *pars triangularis*, gray matter of outer (lateral) wall of sub-gyral fold.; BA45
Pt. B	A2	-20	32	11	IFG, *pars triangularis*, subjacent white matter; BA45
	A3	-25	35	15	IFG, *pars triangularis*, grey matter at fundus of sulcus; BA45
	A4	-30	36	21	IFG, *pars triangularis*, gray matter, middle of sulcus; BA45
Pt. C	B5	-32	30	11	IFG *pars opercularis*, deep gray matter, facing insula; BA44
	B6	-37	30	14	IFG *pars opercularis*, gray/white border; BA44/45
	B7	-41	31	18	IFG *pars triangularis*, gray matter in inferior frontal sulcus; BA45

Table S2: Anatomical location and approximate MNI coordinates (see Methods) for the major electrode contacts in each patient from which primary results (inflectional condition differences) are reported. The anatomical location of each contact was determined directly, from scans of the individual patients, independently of (not based on) the coordinates. The average coordinate across contacts (-30.1±6.7, 32.1±2.4, 17.3±4.7) falls within the deep IFG in the Talairach atlas (*S1*), and corresponds to the general location where fMRI activations in language tasks are typically ascribed to Broca's area.

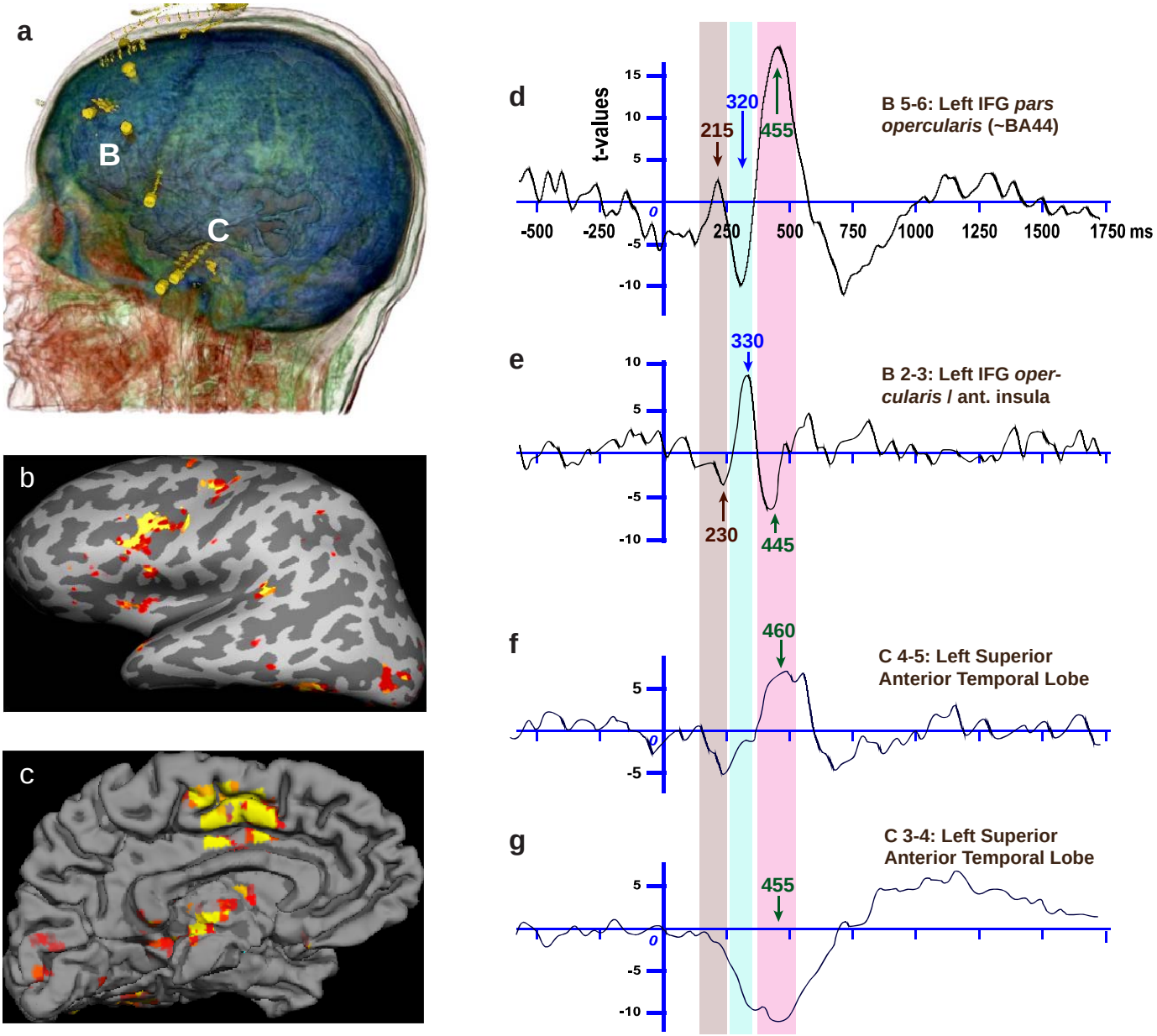

fig. S4. Replication of Broca's area triphasic activity, and slow late temporal-lobe activity, in Patient C. (**a**) Insertion points of depth probes B and C. (**b**,**c**) fMRI activation for this patient, on lateral (inflated) and medial surfaces. Broca's area and the superior temporal lobe showed task-related BOLD activity, in the approximate regions recorded from by probes B and C. fMRI was collected the day before electrodes were implanted. (**d**-**g**) Average all-condition LFP from representative channels, plotted as *t*-scores (paired), showing significant difference from pre-stimulus baseline periods. Broca's area channels recorded the triphasic waveform at nearly the same latencies as in Patient A, while superior temporal lobe channels likewise replicated the late monophasic component. Data were bandpassed between 1Hz and 20Hz.

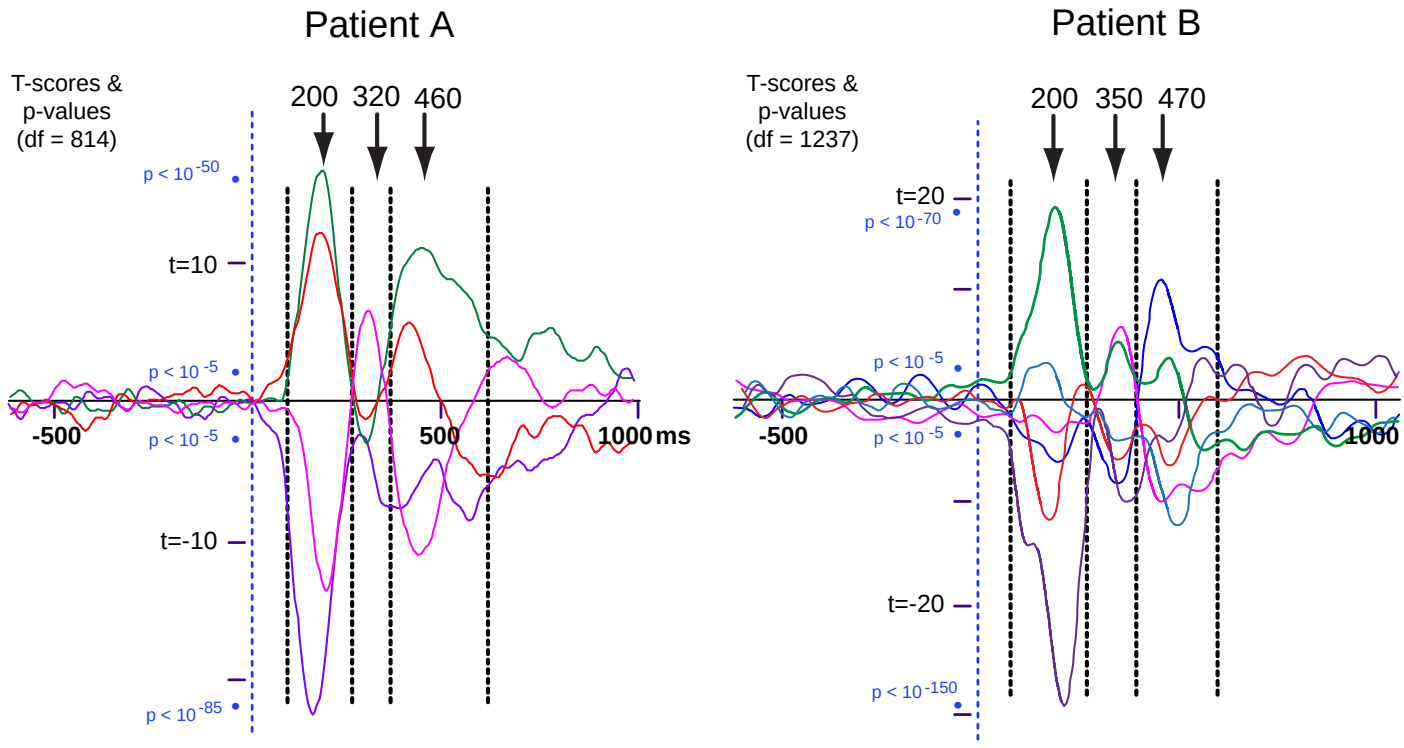

fig. S5. Consistency of the task-related triphasic waveform in patients A and B (patient C is shown in fig. S4). Waveforms and statistical significance levels of the task-related neural activity components are plotted for representative Broca's area channels. Vertical dashed lines, approximate boundaries of the three component epochs. *P*-values are significance levels, corrected for multiple comparisons. Degrees of freedom for *t*-tests for Patient A, 814 (465 task trials, 351 fixation trials), for Patient B, 1237 (704 task trials, 535 fixation trials).

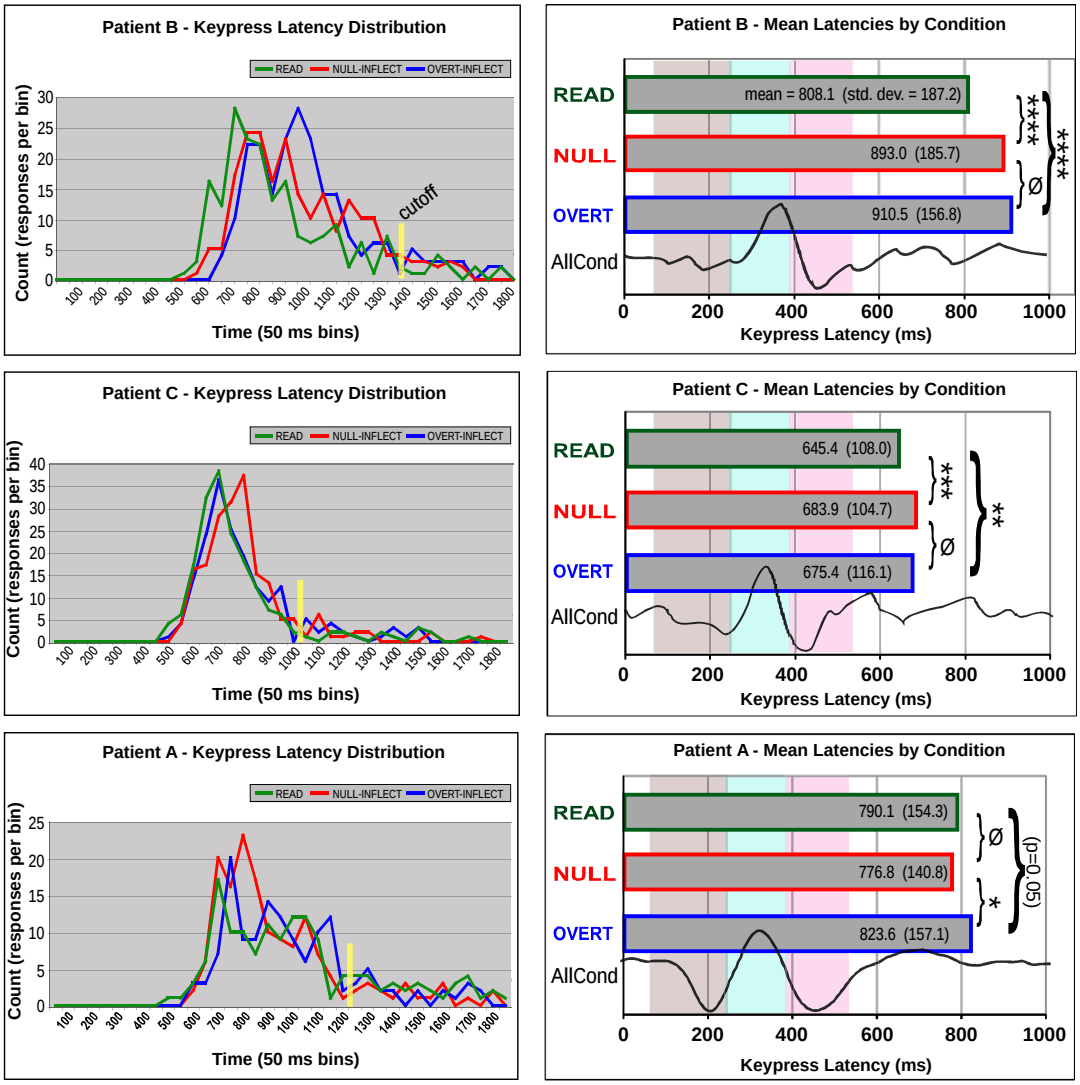

fig. S6. Keypress timings vary by condition and across patients, yet the timing of Broca's area LFP components is constant. **LEFT COLUMN**: For each patient and condition, color-coded plots show the distributions of keypress latencies (time between the onset of the target word and the button-press; see Methods). Time was divided into 50 ms bins and distributions plotted as the number of trials where the keypress latency fell into each bin. All patients and conditions demonstrated a unimodal distribution with a long right tail. We imposed a cutoff at the time bin when all three condition distributions fell below 5 trials per bin (yellow vertical line). **RIGHT COLUMN**: For each patient the mean keypress latency is plotted and the mean and standard deviation annotated. Significant differences among conditions are noted: **** ($P < 0.0001$), *** ($P < 0.001$), ** ($P < 0.01$), Ø (non-significant) (*t*-test: one tail, two-sample, equal variance). Overall, producing inflected words took longer than simply reading them. On the same axes, vertical color bars denote the time windows of the ~200ms lexical, ~320 grammatical, and ~450 phonological LFP components. Superimposed waveform is the average neuronal activity (as LFP) for all conditions from a representative channel. The LFP components occur at nearly the same time across patients and conditions, while the keypress latencies vary widely. This suggests that the mental processes indexed by the components have a fixed timecourse and much of the behavioral variability may accumulate during the final part of each trial – when motor plans for speech must be organized, and further self-monitoring executive processes leading to the keypress are implemented.

S1 J. Talairach, P. Tournoux, *Co-Planar Stereotaxic Atlas of the Human Brain.* (Thieme Medical Publishers Inc., New York, 1988).
S2 N. T. Sahin, S. Pinker, E. Halgren, *Cortex* **42**, 540 (2006).
S3 A. M. Dale, B. Fischl, M. I. Sereno, *Neuroimage* **9**, 179 (1999).
S4 B. Fischl, A. Liu, A. M. Dale, *IEEE Trans. Med. Imaging* **20**, 70 (2001).
S5 B. Fischl, M. I. Sereno, R. B. Tootell, A. M. Dale, *Hum. Brain Mapp.* **8**, 272 (1999).
S6 R. W. Cox, *Comput. Biomed. Res.* **29**, 162 (1996).
S7 A. M. Dale, R. L. Buckner, *Hum. Brain Mapp.* **5**, 329 (1997).
S8 M. A. Burock, A. M. Dale, *Hum. Brain Mapp.* **11**, 249 (2000).
S9 C. R. Genovese, N. A. Lazar, T. Nichols, *Neuroimage*, **15**, 870 (2002).